The Astrophysical Journal Letters, 891:L36 (4pp), 2020 March 10 https://doi.org/10.3847/2041-8213/ab7998

A Nonthermal Bomb Explains the Near-infrared Superflare of Sgr A*

Eduardo M. Gutiérrez[1], Rodrigo Nemmen[2], and Fabio Cafardo[2]
[1] Instituto Argentino de Radioastronomía (IAR, CCT La Plata, CONICET/CIC), C.C.5, (1984) Villa Elisa, Buenos Aires, Argentina; emgutierrez@iar.unlp.edu.ar
[2] Universidade de São Paulo, Instituto de Astronomia, Geofísica e Ciências Atmosféricas, Departamento de Astronomia, São Paulo, SP 05508-090, Brazil
Received 2019 December 20; revised 2020 February 22; accepted 2020 February 24; published 2020 March 12

Abstract

The Galactic center supermassive black hole, Sgr A*, has experienced a strong, unprecedented flare in 2019 May when its near-infrared luminosity reached much brighter levels than ever measured. We argue that an explosive event of particle acceleration to nonthermal energies in the innermost parts of the accretion flow—a nonthermal bomb—explains the near-infrared light curve. We discuss potential mechanisms that could explain this event such as magnetic reconnection and relativistic turbulence acceleration. Multiwavelength monitoring of such superflares in radio, infrared, and X-rays should allow a concrete test of the nonthermal bomb model and put better constraints on the mechanism that triggered the bomb.

Unified Astronomy Thesaurus concepts: Galactic center (565); Black hole physics (159); Non-thermal radiation sources (1119); Accretion (14)

1. Introduction

At the center of the Milky Way lies Sagittarius A* (Sgr A*), a supermassive black hole (SMBH) with a mass of $M = 4 \times 10^6 M_\odot$ located at a distance of 8.2 kpc (Abuter et al. 2019). Given its proximity, Sgr A* presents one of the best laboratories for studying the physics of black hole (BH) accretion flows (Falcke & Markoff 2013). Sgr A* has been detected in most of the electromagnetic spectrum (e.g., Dibi et al. 2014). The extremely low accretion rate and low luminosity observed in its quiescent state ($L_{\rm bol} \sim 10^{36}$ erg s^{-1} $\sim 2 \times 10^{-9} L_{\rm Edd}$ where $L_{\rm Edd}$ is the Eddington luminosity) implies that the accretion flow is in a radiatively inefficient accretion flow (RIAF) state (e.g., Yuan & Narayan 2014).

On top of the quiescent emission, Sgr A* also exhibits frequent flares in X-rays (e.g., Neilsen et al. 2013; Ponti et al. 2015) and near-infrared (NIR; e.g., Genzel et al. 2003; Boyce et al. 2018). About one X-ray flare is seen per day with a typical duration of a few tens of minutes (Neilsen et al. 2013). The brightest observed X-rays flares are ~100 times above the quiescent level (e.g., Nowak et al. 2012). The NIR flares are even more frequent. X-ray flares usually follow the NIR ones after a few tens of minutes, but there are multiple NIR flares without an X-ray counterpart (e.g., Eckart et al. 2006; Yusef-Zadeh et al. 2012; Ponti et al. 2017; but see Fazio et al. 2018). Flares are also observed in millimeter and submillimeter wavelengths (e.g., Yusef-Zadeh et al. 2006; Stone et al. 2016). They last from hours to days with amplitudes of ~25% of the quiescent level (Yusef-Zadeh et al. 2008; Fazio et al. 2018).

In 2019 May, Do et al. (2019) observed an unprecedented NIR flare from Sgr A*—hereafter the "superflare"—with the Keck telescope. The peak flux exceeded the maximum historical value by a factor of two and the light curve (LC) afterward showed a factor of 75 drop in flux over a 2 hr time span. Do et al. (2019) suggested that an increase in the SMBH accretion rate $\dot{M}$ could be responsible for the superflare, possibly due to additional gas deposited by the passage of the G2 object in 2014 or a windy star such as S0-2 in 2018. Nevertheless, Ressler et al. (2018) argued that the effect of S0-2 on the RIAF structure should be negligible. This, combined with the fact that the S-star cluster has no known stars more massive than S0-2 close to Sgr A* spells trouble for the "windy star" scenario.

Here, we propose an entirely different scenario for the superflare that does not rely on an $\dot{M}$-increase: an explosive event of particle acceleration to nonthermal energies in the innermost parts of the accretion flow—a nonthermal bomb. This model explains quantitatively the NIR LC and makes testable predictions at other wavelengths.

2. Model

Our model for the emission involves an RIAF with populations of thermal and nonthermal electrons, following the height-integrated approach of Yuan et al. (2003). For simplicity, we assume that the dynamical structure of the flow (i.e., ρ, $\boldsymbol{v}$, T) does not vary with time, but we consider the possibility that an unspecified acceleration mechanism may change the number of particles following a nonthermal energy distribution.

We take into account the presence of outflows by allowing the accretion rate to decrease with radius as $\dot{M}(r) = \dot{M}_{\rm max}(r/r_{\rm max})^s$ (Blandford & Begelman 1999), with $s = 0.25$. We are only interested in the inner parts of the flow, so we only consider the accretion flow up to $r_{\rm max} = 10^3 r_{\rm S}$ where we set $\dot{M}_{\rm out} \approx 10^{-7} M_\odot$ yr^{-1}. The other parameters are the fraction of turbulent energy directly transferred to electrons $\delta = 0.33$, the viscosity parameter $\alpha = 0.1$, and the gas pressure to magnetic pressure ratio $\beta = 9$.

2.1. Quiescent State

To reproduce the quiescent state of the spectral energy distribution (SED), we assume that in each shell of the RIAF a fraction $\eta_{\rm q} = 0.4\%$ of the thermal energy density of electrons is in a nonthermal population with a broken power-law distribution:

$$N_{\rm q}(\gamma; r) = \begin{cases} K_{\rm q}(r)\,\gamma^{-p}, & \text{if } \gamma_{\rm min} \leqslant \gamma \leqslant \gamma_{\rm c}, \\ K_{\rm q}(r)(p-1)\gamma_{\rm c}\gamma^{-(p+1)}, & \text{if } \gamma_{\rm c} \leqslant \gamma \leqslant \gamma_{\rm max}, \end{cases} \quad (1)$$

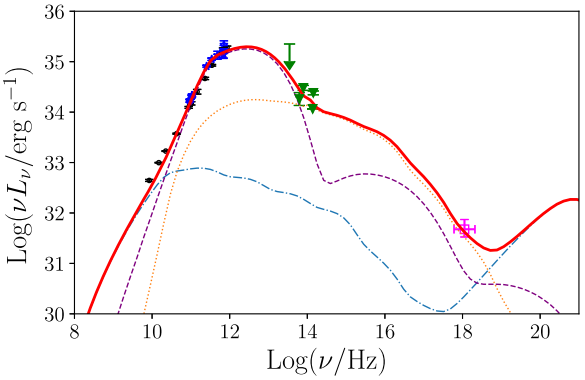

Figure 1. SED of Sgr A* in the quiescent state. The dotted line is the emission of nonthermal electrons from the inner parts of the flow ($r < 15r_S$). The dashed line is the thermal synchrotron and inverse Compton emission. The dotted–dashed line is the emission from the outer parts of the flow ($r > 15r_S$), including thermal bremsstrahlung and nonthermal synchrotron. The solid line is the total emission.

where N_q is the number density of electrons in the quiescent state, γ is the electron Lorentz factor, p is the spectral index at injection, γ_c is the "cooling break" Lorentz factor at which the the accretion time is equal to the cooling time, $t_{acc} = t_{cool}(\gamma_c)$ (cf. Section 4), and γ_{min} and γ_{max} denote the minimum and maximum Lorentz factors, respectively. We assume that thermal electrons radiate locally through synchrotron, bremsstrahlung, and inverse Compton processes. For nonthermal electrons, we only consider synchrotron emission and adopt $p = 3.6$.

Figure 1 shows the quiescent state SED for the parameters given above. The observations are from Liu et al. (2016) (radio, dark circles), Shcherbakov et al. (2012) (radio, blue dots), Schödel et al. (2011) (IR, green triangles), and Roberts et al. (2017) (X-rays, magenta square). The submillimeter bump is due to thermal synchrotron, and the radio and IR excess are nonthermal synchrotron radiation.

2.2. Flare

Our model for flaring emission assumes that an unspecified process converts a fraction of electrons from the Maxwellian distribution to a nonthermal one during a short burst—a "nonthermal bomb." In Section 4 we discuss about the possible physical mechanisms that might have produced such an event.

We consider that the burst occurs over an extended region ranging from radius r_{in} to r_{out}. The injection function of nonthermal particles during a burst is

$$\dot{N}_b(\gamma, r; t) = \dot{N}_b(\gamma, r)\delta(t), \quad (2)$$

where $\dot{N}_b(\gamma, r) = K_b(r)\gamma^{-p_b}$, and $K_b(r)$ is determined imposing that at each shell a fraction $\eta_b > \eta_q$ of the thermal energy goes to nonthermal particles. We follow the population while it is accreted onto the event horizon and compute the time evolution of the synchrotron emission. The transport equation that governs the evolution of this population is

$$\frac{\partial N_b(\gamma, r; t)}{\partial t} + \frac{1}{r^2}\frac{\partial}{\partial r}[r^2 v(r) N_b(\gamma, r; t)] + \frac{\partial}{\partial \gamma}\left[\left(\frac{d\gamma}{dt}\right)_{syn} N_b(\gamma, r; t)\right] = \dot{N}_b(\gamma, r)\delta(t), \quad (3)$$

where $d\gamma/dt(\gamma, r)$ is the rate of energy losses by synchrotron emission and $v(r)$ is the radial velocity of the flow. We solve Equation (3) by the method of characteristics. There are five free parameters in the flare model: η_b, the spectral index p_b, r_{in}, r_{out}, and t_0, which is the time at which the burst occurs.

3. Results

Figure 2 contains the main result of this Letter: we successfully explain the unprecedented bright state of Sgr A* observed in the NIR in 2019 May as an injection burst of nonthermal particles in the RIAF, which subsequently undergo radiative cooling as they get advected onto the BH. The figure shows three models with different initial sizes of the burst region that reproduce well the decay in the NIR emission. The models reproduce the abrupt decrease in the flux in the last 10 minutes of observations. This is interpreted as the accretion of the last nonthermal particles accelerated in the burst—those near r_{out} at $t = 0$.

Our nonthermal bomb model predicts that the duration of the flare—determined by the accretion time—is the same across all wavelengths. The model also predicts that the slope of the LC following the initial burst depends on the wavelength. Both of these features are seen in Figure 3, which shows LCs in three different wavelengths: NIR, 1.3 mm (the Event Horizon Telescope wavelength), and 2–8 keV (the *Chandra* and *XMM-Newton* energy band). The NIR LC is relatively insensitive to the slope of the electron energy distribution function, such that $L_{NIR} \propto t^{-0.7}$. On the other hand, we find that the radio emission at millimeter wavelengths depends modestly on the power-law index p_b. This dependence can be approximated as $L_{mm} \propto t^{0.4-0.25p_b}$. The X-ray LC follows $L_X \propto t^{0.4}$ and depends weakly on p_b. Therefore, a campaign of multiwavelength monitoring of Sgr A*'s LC following a superflare in radio, NIR, and X-rays should allow a concrete test of our model.

Figure 3 also demonstrates that there is more than one combination of parameters capable of reproducing the NIR observations. For instance, the effect of the parameters p_b and η_b on the LC is degenerate: a change in any of these parameters affects only the total luminosity at the K_s band but does not modify the slope of the LC. This degeneracy can be broken by monitoring Sgr A* following the outset of the nonthermal bomb at other wavelengths. A change in η_b only, leaving p_b fixed, modifies the total amount of energy in the bomb, and thus the luminosity at all times and wavelengths. This is shown in Figure 3.

4. Discussion

4.1. Acceleration Mechanism

What is the mechanism responsible for for triggering the nonthermal bomb in Sgr A*? BH accretion flows are highly turbulent, highly magnetized, relativistic environments (e.g., Porth et al. 2019). Thus, plausible culprits are magnetic reconnection events and/or turbulence acceleration. In fact, magnetic reconnection has been invoked to explain the recurring IR and X-ray flares observed in Sgr A* (e.g., Ball et al. 2018). Shocks are unlikely because while being efficient at dissipating energy, they do not accelerate particles far beyond thermal energies (e.g., Sironi et al. 2015).

Numerical solutions of the Vlasov equation for astrophysical plasmas—i.e., particle-in-cell (PIC) simulations—are showing

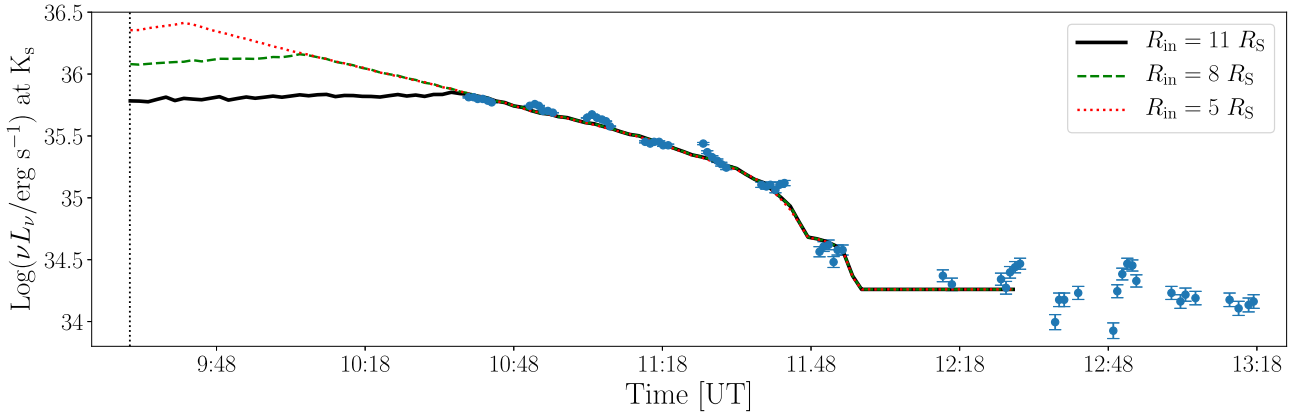

Figure 2. NIR LC of the superflare of Sgr A*. Points correspond to the Keck Telescope observations of Do et al. (2019) and lines indicate different nonthermal bomb models. The model parameters are $\eta_b = 0.25$, $p_{\rm b} = 2.05$, and $r_{\rm out} = 16 r_{\rm S}$, for three different values of $r_{\rm in}$.

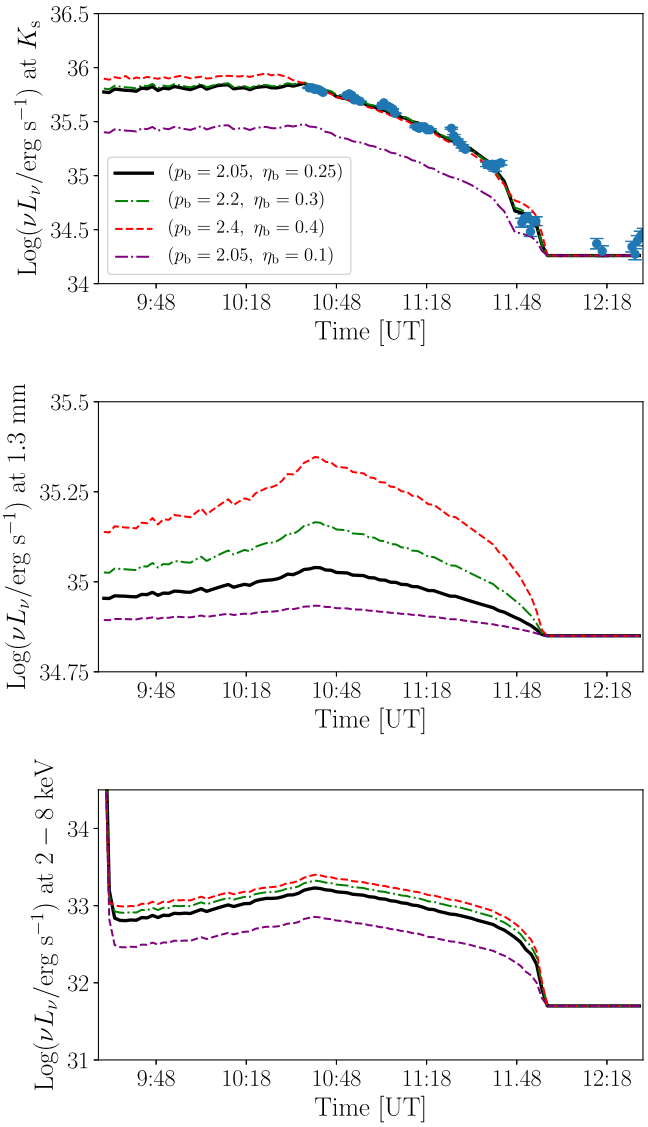

Figure 3. Predicted flare emission at three wavelengths: NIR (upper panel), 1.3 mm (middle panel), and X-rays (2–8 keV; lower panel). Three different values of the spectral index of the nonthermal distribution are displayed plus a model with the same spectral index as our fiducial model but with a lower value of $\eta_{\rm b}$.

that: (i) magnetic reconnection events with high magnetizations[3] of $\sigma \gtrsim 10$ lead to particles following power-law energy distributions with an index p ranging from 1 to 2 (e.g., Guo et al. 2014; Sironi & Spitkovsky 2014), (ii) the presence of relativistic[4] turbulence acceleration leads to a power-law index closer to 2 (Comisso & Sironi 2019), and (iii) reconnection can deposit a large fraction (up to about 50%) of the dissipated energy in nonthermal electrons.

We have found that models with p between 2 and 2.5 and $\eta_b \approx 0.25$ can account for the NIR flare evolution. Energy distributions with these parameters are consistent with having been produced within 10 gravitational radii of the event horizon by either a magnetic reconnection event, or a reconnection event followed by relativistic turbulence acceleration.

For instance, according to the PIC simulations of Petropoulou et al. (2016) a lone reconnection event with $\sigma \approx 10$ should produce nonthermal electrons with the required values of p and $\eta_{\rm b}$. Global GRMHD simulations such as those carried out by Ball et al. (2018) demonstrate that σ is correlated with the plasma-β, $\beta \equiv P_{\rm gas}/P_{\rm magnetic}$. The values of $\sigma \gtrsim 10$ required to explain the superflare are only attained in configurations with high amounts of magnetic flux near the event horizon—i.e., the magnetically arrested disk (MAD) state—in regions of the accretion flow at which $\beta \sim 0.1$ (Ball et al. 2018). In our fiducial LC model, the total amount of magnetic energy involved in the burst is $\sim 3 \times 10^{40}$ erg s^{-1}. The MAD models of Ball et al. reach at most $\sim 10^{39}$ erg s^{-1} for $\sigma \approx 10$; therefore, a nonthermal bomb needs unusually large values of B—three times larger than the peak values of B reached in MAD models. This would explain why superflares such as the one observed in 2019 May should be quite rare.

4.2. Timescales

The relevant timescales for our problem are the electron cooling time and the accretion time. Interestingly, during the nonthermal bomb these timescales should be comparable. The synchrotron cooling time for an electron of Lorentz factor γ is

$$t_{\rm syn} \approx 7.74 \times 10^6 \left(\frac{B}{10\ {\rm G}}\right)^{-2} \gamma^{-1}\ {\rm s}. \quad (4)$$

[3] The magnetization parameter is defined as $\sigma \equiv B^2/4\pi\rho c^2$, where B is the magnetic field intensity and ρ is the mass density—all quantities measured in the rest frame of the fluid.

[4] Hereafter, by relativistic we mean that the mean magnetic energy per particle is larger than the rest-mass energy.

The cooling time corresponds to

$$t_{\rm syn} \approx \left(\frac{B}{10\ {\rm G}}\right)^{-3/2} {\rm hr}. \quad (5)$$

For magnetic fields of the order of 10 G, as appropriate for Sgr A* at $\approx 10 r_{\rm S}$, the cooling time is of the order of one hour. The accretion timescale is defined as $t_{\rm acc} = R/|v|$. Using the self-similar RIAF solution (Narayan & Yi 1994) we obtain a first-order estimate of this timescale as

$$t_{\rm acc} \approx 3\alpha r^{3/2}\ {\rm hr}. \quad (6)$$

For $\alpha = 0.1$ and $r \approx 10$, $t_{\rm acc} \sim 10$ hr. In the models displayed in Figure 2, the duration of the flare is determined mainly by the accretion time, but the slope also depends on the electron cooling. However, we find that a model only taking into account cooling with electrons remaining at a fixed distance from the hole—i.e., undergoing convective motion—also fits well the data. This shows that cooling can have an effect as important as accretion in our model.

5. Summary

Sgr A* has experienced a strong, unprecedented flare in 2019 May when its near-IR luminosity reached much brighter levels than ever measured. We have explained this superflare with a nonthermal bomb model, where an unspecified process accelerates over a very short time a small fraction of the electrons into a nonthermal distribution; these electrons subsequently cool and are advected onto the BH. Besides explaining the NIR LC, our model predicts that the radio and X-ray fluxes should decay over time in a similar fashion. In particular, the radio LC at millimeter wavelengths is sensitive to the particle energy distribution and dissipation efficiency.

The nonthermal bomb detonated in a region spanning a length $5R_S$ in the innermost parts of the accretion flow, and is likely due to a magnetic reconnection event involving unusually strong magnetic fields and high magnetization, i.e., $\sigma \gtrsim 10$, or such a reconnection event followed by turbulence acceleration.

A multiwavelength monitoring of such superflares in radio, NIR, and X-rays should allow a concrete test of the nonthermal bomb model and better constrain the mechanism that triggered the bomb. Future theoretical research should investigate the observational signatures of relativistic reconnection and relativistic turbulence acceleration using realistic magnetic field configurations appropriate for the SMBH in our Galactic Center, combining the tools of multidimensional GRMHD and PIC simulations.

We thank Reinaldo Santos de Limia for useful discussions, Fan Guo for providing us useful references, and the anonymous referee for very constructive comments that led to improvements in this Letter. E.G. thanks Gustavo Romero and Florencia Vieyro for useful discussions about relativistic processes in the vicinity of black holes. This work was supported by the Argentine National Scientific and Technical Research Council (CONICET, grant PIP 2014-00338), the National Agency for Scientific and Technological Promotion (PICT 2017-0898), Fundação de Amparo à Pesquisa do Estado de São Paulo (FAPESP, grant 2017/01461-2), and Conselho Nacional de Desenvolvimento Científico e Tecnológico (CNPq, grant 142320/2016-1).

ORCID iDs

Eduardo M. Gutiérrez https://orcid.org/0000-0001-7941-801X
Rodrigo Nemmen https://orcid.org/0000-0003-3956-0331
Fabio Cafardo https://orcid.org/0000-0002-7910-2282

References

Abuter, R., Amorim, A., Bauboeck, M., et al. 2019, in Proc. XIII Scientific Meeting of the Spanish Astronomical Society, Highlights on Spanish Astrophysics X, ed. B. Montesinos et al. (Berlin: Springer), 609
Ball, D., Özel, F., Psaltis, D., Chan, C.-K., & Sironi, L. 2018, ApJ, 853, 184
Blandford, R. D., & Begelman, M. C. 1999, MNRAS Letters, 303, L1
Boyce, H., Haggard, D., Witzel, G., et al. 2018, arXiv:1812.05764
Comisso, L., & Sironi, L. 2019, ApJ, 886, 122
Dibi, S., Markoff, S., Belmont, R., et al. 2014, MNRAS, 441, 1005
Do, T., Witzel, G., Gautam, A. K., et al. 2019, ApJL, 882, L27
Eckart, A., Baganoff, F. K., Schödel, R., et al. 2006, A&A, 450, 535
Falcke, H., & Markoff, S. B. 2013, CQGra, 30, 244003
Fazio, G. G., Hora, J. L., Witzel, G., et al. 2018, ApJ, 864, 58
Genzel, R., Schödel, R., Ott, T., et al. 2003, Natur, 425, 934
Guo, F., Li, H., Daughton, W., & Liu, Y.-H. 2014, PhRvL, 113, 155005
Liu, H. B., Wright, M. C. H., Zhao, J.-H., et al. 2016, A&A, 593, A107
Narayan, R., & Yi, I. 1994, ApJL, 428, L13
Neilsen, J., Nowak, M. A., Gammie, C., et al. 2013, ApJ, 774, 42
Nowak, M. A., Neilsen, J., Markoff, S. B., et al. 2012, ApJ, 759, 95
Petropoulou, M., Giannios, D., & Sironi, L. 2016, MNRAS, 462, 3325
Ponti, G., De Marco, B., Morris, M. R., et al. 2015, MNRAS, 454, 1525
Ponti, G., George, E., Scaringi, S., et al. 2017, MNRAS, 468, 2447
Porth, O., Chatterjee, K., Narayan, R., et al. 2019, ApJS, 243, 26
Ressler, S. M., Quataert, E., & Stone, J. M. 2018, MNRAS, 478, 3544
Roberts, S. R., Jiang, Y.-F., Wang, Q. D., & Ostriker, J. P. 2017, MNRAS, 466, 1477
Schödel, R., Morris, M. R., Muzic, K., et al. 2011, A&A, 532, A83
Shcherbakov, R. V., Penna, R. F., & McKinney, J. C. 2012, ApJ, 755, 133
Sironi, L., Keshet, U., & Lemoine, M. 2015, SSRv, 191, 519
Sironi, L., & Spitkovsky, A. 2014, ApJL, 783, L21
Stone, J. M., Marrone, D. P., Dowell, C. D., et al. 2016, ApJ, 825, 32
Yuan, F., & Narayan, R. 2014, ARA&A, 52, 529
Yuan, F., Quataert, E., & Narayan, R. 2003, ApJ, 598, 301
Yusef-Zadeh, F., Arendt, R., Bushouse, H., et al. 2012, ApJL, 758, L11
Yusef-Zadeh, F., Roberts, D., Wardle, M., Heinke, C. O., & Bower, G. C. 2006, ApJ, 650, 189
Yusef-Zadeh, F., Wardle, M., Heinke, C., et al. 2008, ApJ, 682, 361